European Journal of Pharmaceutics and Biopharmaceutics 112 (2017) 119–131

Contents lists available at ScienceDirect

European Journal of Pharmaceutics and Biopharmaceutics

journal homepage: www.elsevier.com/locate/ejpb

Research paper

Glycosylation and antiproliferative activity of hyperglycosylated IFN-α2 potentiate HEK293 cells as biofactories

Agustina Gugliotta [a], Natalia Ceaglio [a], Brenda Raud [b], Guillermina Forno [b,c], Laura Mauro [c], Ricardo Kratje [a], Marcos Oggero [a,*]

[a] UNL, CONICET, FBCB, Cell Culture Laboratory, Ciudad Universitaria UNL.C.C. 242, (S3000ZAA) Santa Fe, Argentina
[b] UNL, FBCB, Cell Culture Laboratory, Ciudad Universitaria UNL.C.C. 242, (S3000ZAA) Santa Fe, Argentina
[c] Zelltek S.A., PTLC RN 168, (S3000ZAA) Santa Fe, Argentina

ARTICLE INFO

Article history:
Received 18 March 2016
Revised 22 September 2016
Accepted in revised form 13 November 2016
Available online 17 November 2016

Keywords:
Hyperglycosylated IFN-α2b
N-glycosylation
Glycoproteins
Antitumoral activity
Pharmacokinetics
HEK293 cells
CHO cells

ABSTRACT

Both CHO and HEK cells are interesting hosts for the production of biotherapeutics due to their ability to introduce post-translational modifications such as glycosylation. Even though oligosaccharide structures attached to proteins are conserved among eukaryotes, many differences have been found between therapeutic glycoproteins expressed in hamster and human derived cells. In this work, a hyperglycosylated IFN-α2b mutein (IFN4N) was produced in CHO and HEK cell lines and an extensive characterization of their properties was performed. IFN4N$_{CHO}$ exhibited a higher average molecular mass and more acidic isoforms compared to IFN4N$_{HEK}$. In agreement with these results, a 2-times higher sialic acid content was found for IFN4N$_{CHO}$ in comparison with the HEK-derived protein. This result was in agreement with monosaccharide quantification and glycan's analysis using WAX chromatography and HILIC coupled to mass spectrometry; all methods supported the existence of highly sialylated and also branched structures for IFN4N$_{CHO}$ glycans, in contrast with smaller and truncated structures among IFN4N$_{HEK}$ glycans. Unexpectedly, those remarkable differences in the glycosylation pattern had not a considerable impact on the clearance rate of both molecules in rats. In fact, although IFN4N$_{HEK}$ reached maximum plasma concentration 3-times faster than IFN4N$_{CHO}$, their elimination profile did not differ significantly. Also, despite the *in vitro* antiviral specific biological activity of both proteins was the same, IFN4N$_{HEK}$ was more efficient as an antiproliferative agent in different tumor-derived cell lines. Accordingly, IFN4N$_{HEK}$ showed a higher *in vivo* antitumor activity in animal models. Our results show the importance of an appropriate host selection to set up a bioprocess and potentiate the use of HEK293 cells for the production of a new hyperglycosylated protein-based pharmaceutical.

1. Introduction

Due to the properties that glycosylation confers, it represents the most important attribute of many therapeutic glycoproteins. Glycosylation defines the potency and effectiveness of biopharmaceuticals, since it is involved in protein solubility, stability, immunogenicity and pharmacokinetics [1]. Technically, glycosylation is an enzymatic process in which oligosaccharide structures are transferred to the polypeptide chain and processed later, resulting in the mature glycoprotein. As regards the type of linkage that binds the glycan to the protein, *N*-linked and *O*-linked glycosylation have been described. The first one is a co-translational process that starts in the endoplasmic reticulum (RE) where a block of sugars is transferred to the Asn located in the consensus sequence Asn-Xxx-Thr/Ser of the protein (where Xxx must not be Pro). Subsequently, the glycan structure is remodeled, a procedure that ends in the Golgi. The second type of linkage is a post-translational process that occurs in the Golgi. Briefly, individual monosaccharides are added to residues of Ser or Thr located in an environment rich in Ser, Thr and Pro. In this case, no consensus sequence has been described [1].

Regarding the complexity of the glycosylation process, the structure of carbohydrates attached to proteins is not only determined by the polypeptide structure itself, but it can also be affected by the culture conditions (culture medium composition, temperature, pH, osmolality, among others) and the intrinsic characteristics of the host cell line. In relation to the production of therapeutic glycoproteins intended for use in humans, mammalian cell lines are the chosen hosts since they produce glycan structures

* Corresponding author.
E-mail address: moggero@fbcb.unl.edu.ar (M. Oggero).

http://dx.doi.org/10.1016/j.ejpb.2016.11.012
0939-6411/

similar to the ones found in humans. However, many differences have been found between the glycosidic structures of proteins produced by different mammals [2].

Chinese Hamster Ovary (CHO) cells are the most commonly used mammalian hosts for the production of commercially approved biopharmaceuticals. Since they have been used successfully in adherent and suspension conditions for the production of a large number of proteins, they represent a well characterized and robust system [3,4]. In the last years, human cell lines have emerged as production systems because of their ability to produce glycoproteins bearing post-translational modifications consistent with those seen on endogenous human proteins. Specifically, Human Embryonic Kidney (HEK) cells allow not only the introduction of specific carbohydrate structures (α2-6 sialic acid; α1-3/4 fucose and bisecting GlcNAc) but also the correct cleavage of propetides, γ-carboxylation of glutamic acid residues and sulfation of tyrosines. These modifications are characteristic of human cells but cannot be done by hamster-derived cells due to the absence of certain enzymes [4,5]. Also, CHO cells produce antigenic glycans such as *N*-glycolylneuraminic acid (Neu5Gc) and α-galactose that are not present in human-derived products [6–8]. The presence of circulating antibodies against them in humans may result not only in increased immunogenicity but also in altered pharmacokinetics of these products [9,10]. Even though these antigenic glycans can be controlled, there is an increasing interest in using human cell lines for the production of recombinant therapeutic proteins, especially for those that need specific post-translational modifications. In addition, HEK cells offer the advantage of being easy to grow in suspension serum-free culture and efficiently transfected by diverse methods. In fact, three HEK derived products have been approved by the Food and Drug Administration (FDA) and one by the European Medicines Agency (EMA) [5].

Type I Interferons (IFNs) were first described as cytokines capable of controlling viral infections by blocking the replication of viruses and inducing an antiviral state in the neighbor cells. They can also work as antiproliferative agents since they slow down the growth of cells by inducing or activating pro-apoptotic genes and proteins. In this way, the antiproliferative activity is crucial for the virus response [11–13]. Moreover, immunomodulatory effects have been reported for type I IFNs (IFN-α and -β) since they actively participate during the adaptative and acquired immune responses. The potential of IFN-α as a multifunctional cytokine and its effectiveness have made it an interesting candidate to treat and to prevent viral and cancer diseases in the near future. Despite all the benefits IFN-α therapy can provide, some adverse, severe and chronic effects have been reported when frequent and high doses are administered. The appearance of headaches, malaises, fever, chills and rarely anorexia and depression, limits the dosage of IFN-α [12,14]. For these reasons, the development of IFN-α molecules with longer half-life is crucial in order to decrease the daily frequency of administration.

Different glycoengineering strategies have been designed and successfully implemented in order to improve the pharmacokinetic properties of therapeutic molecules [15]. The fusion of a peptide containing potential *N*- and/or *O*-glycosylation sites to the polypeptide chain, as well as the introduction of potential *N*-glycosylation sites in the protein sequence by modifying certain amino acids have allowed the development of new therapeutics. In our laboratory, a hyperglycosylated IFN-α2b analog has been generated and produced in CHO-K1 cells. It has been called IFN4N since it has four potential *N*-glycosylation sites which were introduced by point mutations in its protein sequence. As a result of the increment of the glycosylation degree, IFN4N showed increased molecular mass and charge in comparison with the unmodified molecule, resulting in an improvement in its pharmacokinetic properties. Despite IFN4N has lower *in vitro* activity, it showed a better performance in *in vivo* animal models of prostate cancer in comparison with the non-glycosylated IFN [16].

The attractive properties demonstrated by IFN4N prompted us to develop not only CHO-K1 but also HEK293 producer cell lines, in order to investigate the differences in the carbohydrate composition of both products as well as its influence on their *in vitro* biological activity, pharmacokinetics and *in vivo* bioactivity in rodent models.

Here we report the production, purification and characterization of the hyperglycosylated IFN-α2b mutein (IFN4N) produced in CHO-K1 and HEK293 cells. Comparative analysis of both molecules was performed. To our knowledge, this is the first report that describes the potentiality of using the human cell line HEK over the rodent model CHO in terms of the overall analysis of glycosylation, *in vitro* biological activity, pharmacokinetics and *in vivo* bioactivity for the production of a new biopharmaceutical exhibiting a high degree of complexity in its glycosylation profile.

2. Methods

2.1. Cell lines

Madine Darby bovine kidney (MDBK) cells were grown in minimum essential medium (MEM; Gibco, USA) supplemented with 10% (v/v) fetal bovine serum (FBS; Gibco, USA) (growth medium). For bioassays, MEM supplemented with 2% (v/v) FBS (assay medium) was employed.

The human Burkitt's lymphoma derived cell line (Daudi) was maintained in RPMI 1640 medium (Gibco, USA) plus 10% (v/v) FBS. For bioassays the same medium was employed.

Human malignant melanoma derived cells (A375) were grown in a 1:1 mixture of Dulbecco's Modified Eagle Medium/Ham's Nutrient Mixture F-12 formulation (DMEM/F12; Gibco, USA) supplemented with 10% (v/v) FBS.

Human renal cell carcinoma derived cell line (ACHN) was cultivated in MEM plus 10% (v/v) FBS.

Prostate cancer derived cells (PC-3) were maintained in a 1:1 mixture of RPMI 1640 medium/Ham's F12 supplemented with 10% (v/v) FBS.

All cell lines were incubated at 37 °C in humidified 5% CO_2.

2.2. CHO-K1 and HEK293 IFN4N producer clones

The CHO-IFN4N-P1B8 and HEK-IFN4N-P2A5 adherent cell clones were obtained from the recombinant cell lines generated by lentiviral transduction and subsequent puromycin selection as described previously. Their specific productivity was 817 ± 134 ng $\cdot 10^6$ cell^{-1} day^{-1} and 1490 ± 332 ng $\cdot 10^6$ cell^{-1} day^{-1} of IFN4N, respectively [17].

2.3. IFN4N production

IFN4N was produced by CHO-K1-P1B8 clone ($IFN4N_{CHO}$) and HEK-P2A5 clone ($IFN4N_{HEK}$) using 175 cm^2 T-flasks. Cells were seeded at a density of 250,000 cells ml^{-1} and when the culture reached the maximum confluence, growth medium (DMEM/Ham's F12 5% (v/v) FBS for CHO-K1 cells and DMEM plus 10% (v/v) FBS for HEK 293 cells) was replaced by production medium (containing 0.5% FBS). Harvests were collected every 48 h and replaced by fresh medium. Two production rounds were performed in order to obtain two different batches of each protein.

2.4. IFN4N purification

A specific monoclonal antibody anti-rhIFN-α2b (mAb CA5E6) developed previously in our laboratory [18] was able to recognize

and capture both $IFN4N_{CHO}$ and $IFN4N_{HEK}$ molecules. For this reason, purification of both variants was carried out by immunoaffinity chromatography, using the same resin-coupling procedure, purification method and concentration/diafiltration procedures described by Ceaglio et al. [16]. Several purification rounds were performed from harvests collected during each production round and finally pooled to generate one batch.

2.5. Physicochemical characterization

2.5.1. SDS-PAGE

$IFN4N_{CHO}$ and $IFN4N_{HEK}$ electrophoretic profile were analyzed using 15% (w/v) polyacrylamide resolving gels and 5% (w/v) stacking gels. The purified proteins were diluted in reducing buffer containing 5% (v/v) beta-mercaptoethanol (J.T. Baker®, USA). Separation was performed at 200 V for 75 min. Gels were stained with Coomassie blue and destained with a solution containing 15% (v/v) methanol and 10% (v/v) acetic acid.

2.5.2. IEF

In order to separate the different isoforms of $IFN4N_{CHO}$ and $IFN4N_{HEK}$ a 1-mm thick gel containing 8% (w/v) acrylamide and 7 M urea was prepared. The pH range was established using 70% (w/v) 2–4 ampholytes and 30% (w/v) 5–7 ampholytes. The gel was prefocused at 10 W, 2000 V and 100 mA for 1 h. Then, 10 µl of the samples were applied over a sample application strip placed at 1 cm from cathode. Electrophoresis was carried out using the same conditions as the prefocusing step during 45 min. Finally the gel was stained using a Coomasie blue colloidal solution.

E. coli-derived rhIFN-α2b (Gemabiotech, Argentina) and wild type IFN produced in CHO-K1 cells [19] were used as standards for both methods.

2.6. Biological characterization

2.6.1. In vitro antiviral and antiproliferative biological potency assays

The antiviral and antiproliferative activities of $IFN4N_{CHO}$ and $IFN4N_{HEK}$ were determined *in vitro* using potency-based assays that measure the response of the analytes in comparison with a standard.

The biological antiviral activity of rhIFN-α2b was determined by its ability to inhibit the cytopathic effect caused by vesicular stomatitits virus (VSV) on MDBK cells [20]. For this, MDBK cells were seeded into culture microtiter plates (Greiner, Germany) in growth medium (2.5×10^4 cells per well) and incubated at 37 °C overnight. After removing culture supernatants, 1:2 serial dilutions of rhIFN-α2b WHO international standard (NIBSC 95/566, UK) from 20 IU ml^{-1} to 0.16 IU ml^{-1} or 1:2 serial dilutions of rhIFN-α2b variants test samples in assay medium were added. Plates were incubated for 6 h at 37 °C and, after removal of supernatants, an appropriate dilution of VSV virus was added. Virus replication was allowed to proceed until the cytopathic effect was clearly observable in control wells (no IFN). The medium was discarded and cells were fixed and stained simultaneously with a solution of 0.75% (w/v) crystal violet in 40% (v/v) methanol. After 15 min, plates were washed with water and the remaining dye was solubilized in 20% (v/v) acetic acid. The plates were read at 540 nm with a microtiter plate reader.

The biological antiproliferative activity of rhIFN-α2b was determined by measurement its ability to inhibit growth of Daudi cells [21]. Serial 1:2 dilutions of rhIFN-α2b WHO international standard from 100 IU ml^{-1} to 0.39 IU ml^{-1} or rhIFN-α2b variants test samples were placed into microtiter plate wells. Then, previously washed Daudi cells were added (5×10^3 cells per well) and plates were incubated at 37 °C for 96 h. Cell proliferation was determined using a CellTiter 96™ AQueous Non-Radioactive Cell Proliferation Assay (Promega, USA). Absorbance was read at 492 nm using a microplate reader.

For both experiments, absorbance of the standard and samples were plotted against concentration or dilution, respectively, and the potency of each sample was calculated. Both assays were repeated 5 times and triplicates of the samples were evaluated in each test. Statistical analysis of results was performed using Student's *t* test.

2.6.2. In vitro antiproliferative assays in solid tumor derived cell lines

Further analysis of the antiproliferative activity of $IFN4N_{CHO}$ and $IFN4N_{HEK}$ was performed using three solid tumor derived cell lines: ACHN, A375 and PC-3.

Briefly, twelve 1:2 serial dilutions of each IFN variant starting from 20 µg ml^{-1} were placed into 96-well microtiter plates. Then, exponentially growing cells were harvested and seeded at a density of 4×10^4 cells per well. Cells without treatment were used as a growth control. After 96 h of incubation, cell proliferation was determined as described previously. Samples were analyzed in triplicates. Absorbance values were plotted against protein concentration and the concentration of $IFN4N_{CHO}$ and $IFN4N_{HEK}$ necessary to achieve 50% of cell growth inhibition (IC_{50}) was calculated for each cell line. The experiment was repeated three times and triplicates of each sample were performed.

2.7. Analysis of glycosylation

2.7.1. Sialic acids quantification

Sialic acids were released from native and *N*-deglycosylated IFN variants by acid hydrolysis using 2 M acetic acid at 80 °C during 2 h. For fluorescent labeling, 100 µl of 7 mM 1,2-diamino-4,5-met hylenedioxybenzene (DMB) were added to 200 µl (25 µg) of the hydrolyzed sample. The mixture was incubated in the dark at 50 °C during 3 h. Samples were analyzed in a C18 Jupiter column (Phenomenex, USA) connected to a HPLC system (Waters, USA) equipped with a fluorescence detector module (λ_{exc} = 373 nm, λ_{em} = 448 nm). Elution was performed at 0.9 ml min^{-1} using a mobile phase which consisted on a ratio of 5:7:88 (v/v) of acetonitrile-methanol-water. Samples were analyzed in triplicates. Identification and quantification of different sialic acids was accomplished by comparison with calibration curves constructed using *N*-acetylneuraminic (Neu5Ac) and *N*-glycolylneuraminic (Neu5Gc) acid standards (Calbiochem, France).

2.7.2. Monosaccharide composition

Type and amount of monosaccharides present in $IFN4N_{CHO}$ and $IFN4N_{HEK}$ glycans were determined by acid hydrolysis of the samples followed by high-pH anion-exchange chromatography with pulsed amperometric detection (HPAEC-PAD) using a DIONEX ICS-5000 system equipped with a CarboPac™ PA20 column (Thermo Scientific Dionex, USA). Briefly, 30 µg of each glycoprotein were hydrolyzed with 2 M trifluoroacetic acid (for neutral sugars detection including Gal, Man, Glc, and Fuc) or 6 M HCl (for amino sugars detection including GalNAc and GlcNAc) during 3 h at 100 °C. Then, reaction tubes were cooled down at room temperature, the reaction mixture was dried using Concentrator Plus (Eppendorf, Germany) and dried samples were resuspended in high purity water. Elution was accomplished with 12 mM NaOH followed by 200 mM NaOH to regenerate the column. Monosaccharide mix standard solutions (CM-Mono-Mix-10, Ludger, UK) were treated like sample solutions and used for the identification and quantification of peaks deriving from glycoproteins samples.

2.7.3. N-deglycosylation and fluorescent labeling with 2-aminobenzamide (2-AB)

20 µg of the purified proteins were mixed with 15 mIU of PNGase F (New England Biolabs, UK) in a total volume of 20 µl and incubated at 37 °C ON. Samples were analyzed using

SDS-PAGE followed by Coomasie blue staining in order to verify the complete digestion of both samples.

N-glycans released after the enzymatic digestion were incubated with 5 µl of 0.76 M 2-AB fluorophore labeling solution (Sigma Aldrich, USA) during 2 h at 65 °C. In order to remove 2-AB excess, ascending paper chromatography in acetonitrile using Whatmann 3 MM paper strips was performed. Afterwards, glycans were eluted from the dried paper with water. Samples were filtered using 0.45 µm PDVF filters (Millex, Millipore, France), evaporated and finally resuspended in 30 µl of water for evaluation.

2.7.4. Weak anion exchange chromatography (WAX) for charged labeled N-glycans analysis

To analyze the relative amount of neutral, mono-, bi-, tri- and tetrasialylated structures of $IFN4N_{CHO}$ and $IFN4N_{HEK}$, weak anion exchange (WAX) chromatography was performed. The 2-AB labeled samples were injected in an ASAHIPAK ES-502N7C column (100 × 7.5 mm; SHODEX, Japan) connected to a HPLC system equipped with a fluorescence detector module (λ_{exc} = 330 nm, λ_{em} = 420 nm). A fetuin *N*-glycan standard was used for the identification of the different charged groups. The analysis of the samples was performed twice.

2.7.5. Hydrophilic interaction liquid chromatography (HILIC-UPLC) and mass spectrometry of labeled N-glycans

Analysis of the labeled *N*-glycans was performed on a Waters Acquity UPLC Glycan BEH Amide Column (2.1 mm × 150 mm, 1.7 µm particle). Instrumentation used included an Acquity UPLC Bio-Class H system with a fluorescence detector set at λ_{exc} = 330 - nm; λ_{emis} = 420 nm (Waters Corporation, Milford, MA, USA) and a quadrupole time-of-flight mass spectrometer Synapt G2-Si (Waters Corporation, Milford, MA, USA). The labeled *N*-glycans were separated using typical mobile phases of 100 mM ammonium formate 100 mM pH 4.5, prepared in MS-grade water (solvent A) and 100% ACN (solvent B). The gradient was set from 72 to 52% solvent B over 100 min at a flow rate of 0.2 ml min^{-1} and a column temperature of 40 °C. The mass spectrometer parameters were set with a positive ion V mode. The desolvation gas and source temperature were set to 400 °C and 100 °C, respectively. The capillary and cone voltages were set at 3200 and 30 V, respectively. The *m*/*z* scan range was set to 800–1600. The deconvolution of ESI *m*/*z* mass spectra to calculate MW of the different ions was performed by Mass Biopharmalynx software. Assignment of *N*-glycan structures was performed by comparison between the *m*/*z* observed and the theoretical one.

A dextran ladder (Sigma Aldrich, USA) labelled with 2-AB was also injected in the HILIC column and used for the construction of a calibration curve consisting on glucose units (GU) versus retention time. For each individual peak present in the samples, GU were quantified regarding the calibration curve and possible *N*-glycan structures were assigned by comparing to the ones reported in the GLYCOBASE (National Institute for Bioprocessing Research and Training, Dublin, Ireland) and the literature [22–25].

2.7.6. Exoglycosidases digestion of labeled N-glycans and HILIC-HPLC analysis

2-AB labeled glycans were subjected to digestion using different arrangements of the following enzymes at the indicated concentrations: *Arthrobacter ureafaciens sialidase* (ABS, EC 3.2.1.18, specificity for α2–3, 2–6 and 2–8-linked sialic acid, Biolabs, USA), 50 U ml^{-1}; Bovine testes β-galactosidase (BTG, EC 3.2.1.23, specificity for β1,3/4-linked galactose, Sigma Aldrich, USA), 0.2 U ml^{-1}; jack bean β-*N*-acetylhexosaminidase (JBH, EC 3.2.1.52, specificity for β1,2/3/4/6-linked *N*-acetylglucosamine, Prozyme, USA), 6 U ml^{-1}, bovine kidney α-L-fucosidase (BKF, EC 3.2.1.51, specificity for α1–2,3,4,6 linked fucose, Sigma Aldrich, USA), 0.9 U ml^{-1}. Digestions were performed in 50 mM sodium acetate buffer, pH 5.5 at 37 °C for 18 h. After hydrolysis, *N*-glycans were analyzed by HILIC using a TSK gel Amide 80 column (4.6 × 250 mm; Tosoh Biosciences, Japan) connected to a HPLC system equipped with a fluorescence detector module (λ_{exc} = 330 nm, λ_{em} = 420 nm). For separation, a gradient was applied using two mobile phases consisting in 50 mM formic acid adjusted to pH 4.4 with ammonia solution (solvent A) and acetonitrile (solvent B). Glycan structures assignment was performed using a dextran ladder calibration curve as mentioned in Section 2.7.5.

2.7.7. Reverse phase interaction liquid chromatography (RP-UPLC) coupled to UV and mass spectrometer detectors

Analysis of intact *N*-deglycosylated proteins was performed on a quadrupole time-of-flight mass spectrometer Synapt G2-Si (Waters Corporation, Milford, MA, USA). An Acquity UPLC Bio-Class H system (Waters Corporation, Milford, MA, USA), with UV detector (215 nm) was coupled to the mass spectrometer as an inlet system. The protein was separated on an Acquity BEH UPLC C4 column (2.1 mm × 50 mm, 1.7 µm) using typical mobile phases of 0.1% (v/v) formic acid in MS-grade water (solvent A) and 0.1% (v/v) formic acid in ACN (solvent B). The gradient was set from 20 to 55% solvent B over 22.5 min at a flow rate of 0.15 ml min^{-1} and a column temperature of 30 °C. The mass spectrometer parameters were set in positive ion V mode, with desolvation gas and source temperature were set to 400 °C and 115 °C, respectively. The capillary and cone voltages were set at 3000 and 10 V, respectively. The *m*/*z* scan range was set to 800–2000. The deconvolution of ESI mass spectra of the intact protein was performed by Mass Biopharmalynx software. Assignment of *O*-glycoprotein structures was performed by comparison between the *m*/*z* observed and the theoretical one.

2.8. Pharmacokinetic studies in rats

The pharmacokinetic profiles of $IFN4N_{CHO}$ and $IFN4N_{HEK}$ were analyzed using *in vivo* assays performed in Wistar rats (Comisión Nacional de Energía Atómica, Argentina). Animals were housed in a temperature-controlled room at 23 °C, with a 12 h light/dark cycle and free access to food and water. Rats with an average body weight of 200 g were randomly divided into two groups of eight rats each. Animals were kept under identical experimental conditions except for treatment, so that a completely randomized design could be applied. A unique dose 2×10^5 IU of IFN (determined by the antiviral assay) in a total volume of 200 µl was injected subcutaneously to each rat. The first group was treated with $IFN4N_{HEK}$ while the second one received the CHO-derived molecule. Blood samples were taken at different times of post-injection. To minimize the impact of blood withdrawing, rats from the same group were subdivided into two groups of four rats, so that at each time point a different subgroup of rats was employed for blood extraction (four replicates per time). Blood was collected on heparin, centrifuged at 5000 rpm during 5 min and stored at −20 °C until analysis. Samples were assayed for IFN antiviral activity using the *in vitro* assay described above.

All animal experimental protocols were in accordance with the UK Animals (Scientific Procedures) Act of 1986 and associated guidelines, EU Directive 2010/63/EU, and efforts were made to minimize the number of animals used and their suffering.

Plots of rhIFN-α2b biological activity versus time were constructed for each animal and pharmacokinetic parameters were calculated from these plots [26], considering a mono-compartmental model. The method of residuals, using Microcal Origin software version 5.0 (Microcal Software, USA) was applied for the calculation of maximum plasma concentration (C_{max}), time to reach the C_{max} (T_{max}), terminal half-life ($t_{1/2}$) and apparent

plasma clearance (CL_{app}). Differences between treatments were evaluated through parametric *t*-tests. Comparison of T_{max} was performed using non-parametric Wilcoxon-Mann-Whitney test. Parameters were considered significantly different when $p < 0.05$. Statistical analyses were performed using GraphPad Prism for Windows, version 5.01 (GraphPad Software Inc.). A 90% confidence interval (CI) for the ratio of geometric means was calculated for all the pharmacokinetic parameters; samples were considered bioequivalent when the CI was between 0.8 and 1.25 (bioequivalence criteria).

2.9. In vivo antitumor activity

In vivo bioactivity of rhIFN-α2b was studied as its ability to reduce growth of solid tumors subcutaneously implanted in immunodeficient mice. PC-3 cell line was used to generate a subcutaneous carcinoma model. Tumor cells were harvested from subconfluent cultures, washed once in serum-free medium and resuspended in sterile phosphate-buffered saline (PBS).

Athymic nude homozygous (nu/nu) mice (Comisión Nacional de Energía Atómica) aged between 8 and 10 weeks were maintained under specific pathogen-free conditions in a biological safety cabinet, with a 14–10 h light/dark cycle and a controlled temperature of 28 ± 1 °C. Mice received a subcutaneous injection of 2×10^6 PC-3 cells under the left rear flank. Two days after implantation of tumor cells, mice were randomized into three groups (n = 6) for treatment. Each group received a peritumoral injection of 5 μg of $IFN4N_{CHO}$ or $IFN4N_{HEK}$ once per week. The control group received PBS injections. Tumor size was measured with a caliper every week prior to treatment. After five weeks of treatment, mice were killed and the tumors were excised and weighed. Differences between treatments were assessed using a one-way ANOVA ($p < 0.05$) and a post hoc Tukey's multiple comparison test ($p < 0.05$).

3. Results

3.1. Production and immunoaffinity purification of $IFN4N_{CHO}$ and $IFN4N_{HEK}$

Two batches of $IFN4N_{HEK}$ and $IFN4N_{CHO}$ were generated from different production rounds. The productivity of $IFN4N_{HEK}$ batches was 4.3 μg of purified protein per ml of harvest while the one corresponding to $IFN4N_{CHO}$ varied between 4.3 and 4.6 μg of purified protein per ml of harvest. Several purification procedures were performed to generate one batch from each production round, yielding mean recovery values of 76% and 96% for $IFN4N_{HEK}$ and 74% and 100% for $IFN4N_{CHO}$ batches. Purities of all batches were higher than 92% (Table S1). Consistency of both batches of the two molecules was observed regarding physicochemical, biological and glycosidic properties (Tables S1 and S2), so that average values are shown in the subsequent sections.

3.2. Physicochemical and biological characterization of $IFN4N_{CHO}$ and $IFN4N_{HEK}$

SDS-PAGE and IEF followed by Coomasie blue staining were performed in order to analyze their apparent molecular mass and isoform distribution (Fig. 1). Both assays showed clear differences between the CHO- and HEK-derived IFN4N. The apparent average molecular mass of $IFN4N_{CHO}$ was higher compared to that of $IFN4N_{HEK}$ (Fig. 1a, lanes 4 and 6), with glycoforms ranging from 20.4 to 56.8 kDa for $IFN4N_{CHO}$ and from 20.4 to 49.9 kDa for $IFN4N_{HEK}$ (Table S1). PNGase F digestion of both molecules demonstrated that the differences between the molecular mass of both proteins were mainly due to *N*-glycosylation. These results were also supported by those obtained by IEF (Fig. 1b). Despite both molecules showed a wide diversity of glycoforms, $IFN4N_{CHO}$ demonstrated a lower mean pI as its isoforms were mainly concentrated in the acidic zone of the gel. Contrarily, isoforms from $IFN4N_{HEK}$ were more homogeneously distributed along the entire pH separation range (pI 2.8–4.9), with a smaller proportion of glycoforms situated in the more acidic zone compared to $IFN4N_{CHO}$.

In vitro bioassays showed that antiviral SBAs of $IFN4N_{CHO}$ (65 ± 15 UI ng^{-1}) and $IFN4N_{HEK}$ (65 ± 20 UI ng^{-1}) were indistinguishable (Fig. 2a). However, markedly differences were found after antiproliferative activity analysis (Fig. 2b). Particularly, the antiproliferative SBA of $IFN4N_{CHO}$ was nearly 2 times lower than the value obtained for $IFN4N_{HEK}$ (3.0 ± 0.6 UI ng^{-1} vs. 5.8 ± 0.9 UI ng^{-1}, respectively). The differences between the antiproliferative activities of $IFN4N_{CHO}$ and $IFN4N_{HEK}$ were confirmed by additional analyses performed in three different tumor-derived cell lines: ACHN, A375 and PC-3. The most sensitive cell line to IFN4N treatment was PC-3, followed by A375 and ACHN. Even though both proteins were able to inhibit cell proliferation, $IFN4N_{HEK}$ was more efficient than $IFN4N_{CHO}$ in all the cell lines evaluated. Notably, in all cases a higher mass of $IFN4N_{CHO}$ was necessary to reach the same effect achieved by $IFN4N_{HEK}$. For ACHN cells the effect of both proteins was markedly different (Table 1).

3.3. Glycosidic characterization of $IFN4N_{CHO}$ and $IFN4N_{HEK}$

As it was shown above, glycosydic structures seem to have the main responsibility for the differences observed between the apparent molecular mass of $IFN4N_{CHO}$ and $IFN4N_{HEK}$. Since the potential sites of glycan attachment for both proteins are the same, such differences might be due to the glycan's structure itself (micro-heterogeneity) [27]. Furthermore, significant differences have been described between the glycosylation pattern of therapeutic proteins produced in CHO and HEK cells [28–30].

3.3.1. Sialic acids quantification

Sialic acids are important since they contribute to prolong the half-life of the glycoproteins, avoiding their rapid clearance. However, it is necessary to control the amounts of the immunogenic Neu5Gc among the glycans when the glycoprotein is produced using a non human host in order to avoid therapy failure [8].

The sialic acid content of the CHO-derived molecule was about 2 times higher than the corresponding one for the HEK-derived protein (10.7 ± 0.6 vs. 4.7 ± 0.4 mol of Neu5Ac per mol of protein, respectively). This result was in accordance with that of the IEF assay where a higher proportion of acidic isoforms were detected for $IFN4N_{CHO}$ in comparison with $IFN4N_{HEK}$. Considering a detection limit of the assay of 34 mmol of Neu5Gc per mol of protein, it is important to note that no detectable amounts of Neu5Gc were found in $IFN4N_{HEK}$, while a 1.1% of Neu5Gc (0.12 ± 0.02 mol per mol of protein) was detected for $IFN4N_{CHO}$.

In order to distinguish the sialic acids coming from *N*- or *O*-glycosylation sites, the quantification of this monosaccharide from *N*-deglycosylated IFN4N variants was performed. The results indicated that Neu5Ac content was also around 2 times higher for the CHO-derived *O*-glycosylated IFN4N than the corresponding one for the HEK-derived *O*-glycoprotein (2.4 ± 0.5 vs. 1.0 ± 0.1 mol of Neu5Ac per mol of protein, respectively). The same degree of sialic acid contribution from *O*-glycans regarding the total content of the same residue (22% from CHO and 21% from HEK-derived IFN4N) was observed for both proteins, i.e., not only *N*-glycans but also *O*-glycans produced by HEK cells were less sialylated.

3.3.2. Monosaccharide composition analysis

The quantification of amino and neutral monosaccharides revealed that CHO and HEK-derived IFN4N proteins exhibit similar

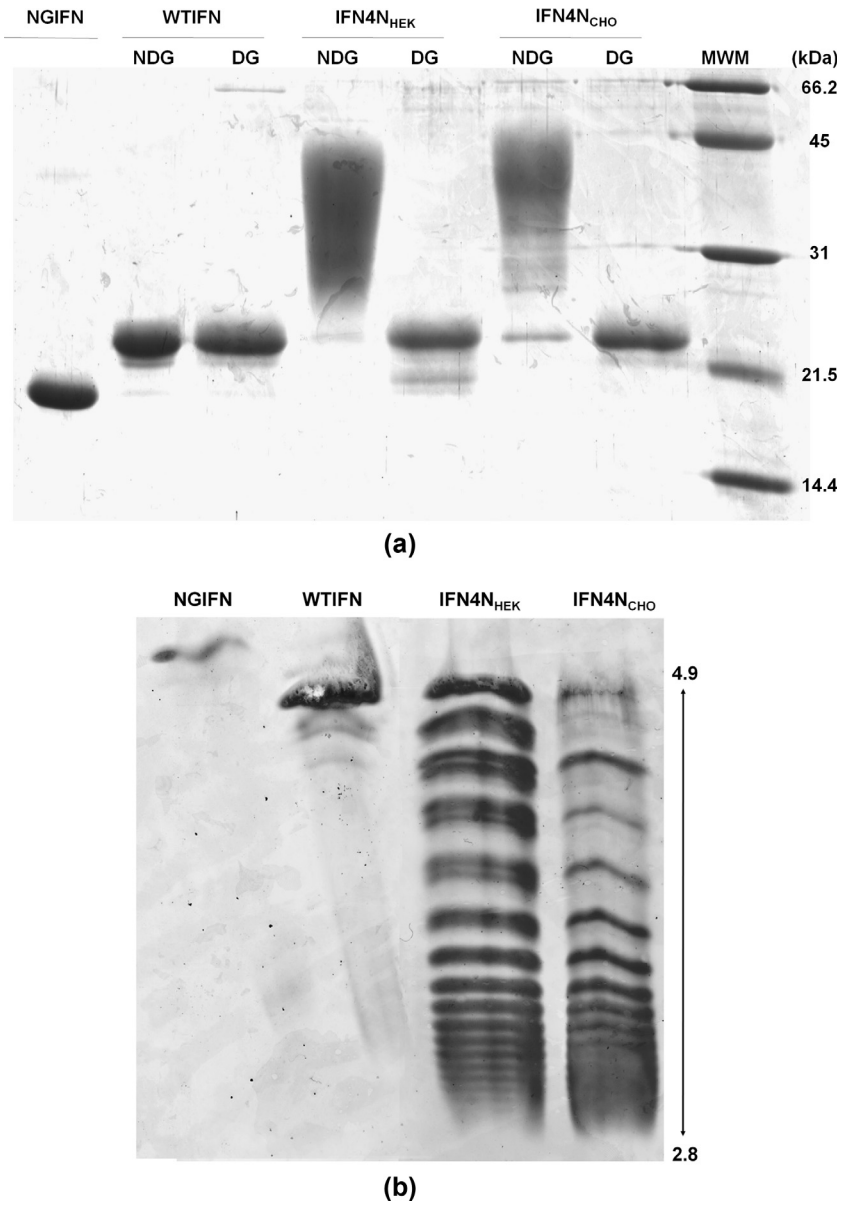

Fig. 1. (a) SDS-PAGE of *N*-deglycosylated (DG) and non-deglycosylated (NDG) IFN4N$_{CHO}$ and IFN4N$_{HEK}$. Non-glycosylated IFN (NGIFN), wild-type IFN (WTIFN) and molecular mass standards (MWM, BioRad) were used as controls. (b) IEF profiles of CHO and HEK-derived IFN4N glycoforms. Arrows indicate the range of pH employed.

amounts of GlcNAc, GalNAc, Man and Fuc. However, Gal content was 3.7 times higher for IFN4N$_{CHO}$ (Table 2), indicating that glycans attached to this IFN variant might be more branched than the ones isolated from IFN4N$_{HEK}$. Also, truncated glycosidic structures might be present among HEK glycans.

Besides, the presence of similar quantities of GalNAc in both variants owes to the natural O-glycosylation that occurs in the Thr106 of hIFN-α2b.

3.3.3. Comparison of the neutral and charged N-glycans

WAX-HPLC was performed to separate the labeled *N*-glycans according to their charge. For both molecules, glycans containing from zero to four sialic acids were identified using a fetuin standard (Fig. 3). IFN4N$_{HEK}$ exhibited a high proportion of neutral and monosialylated structures, while IFN4N$_{CHO}$ glycans comprised mainly bi-, tri- and tetrasialylated species. 49% of the glycan structures detected for IFN4N$_{HEK}$ were neutral, 19% were monosialylated, 14% were bisialylated, 9% were trisialylated and 7% were tetrasialylated. For IFN4N$_{CHO}$ only 6% of the structures were neutral while the remaining were mono-, bi-, tri- and tetrasialylated (11, 23, 30 and 26% respectively). Both samples exhibited a group of peaks eluting at the same retention time than high mannose 5- and 6-phosphate (HMP) glycan standards, corresponding to 4% for IFN4N$_{CHO}$ and 2% for IFN4N$_{HEK}$. HMP bearing proteins can be bound and transported by the mannose phosphate receptor to lysosomes [31] and have been found in marketed therapeutic glycoproteins expressed in CHO cells [32]. A previous report showed that 3.1% of HMP was found among IFN4N$_{CHO}$ glycans using HPAEC-PAD analysis [33].

On the one hand, it was notable that, for IFN4N$_{CHO}$, the most abundant peak from the groups bearing 1, 2, 3 or 4 sialic acids was the one at the last position (from left to right) of each group, corresponding to mono-, bi-, tri- and tetraantennary structures completely substituted with sialic acid residues, respectively. The other peaks observed for each group can be attributed to larger glycans with the same degree of sialylation and, more specifically, to glycan structures bearing *N*-acetyllactosamine repeats (LacNAc) and structures of higher antennarity but not completely sialylated.

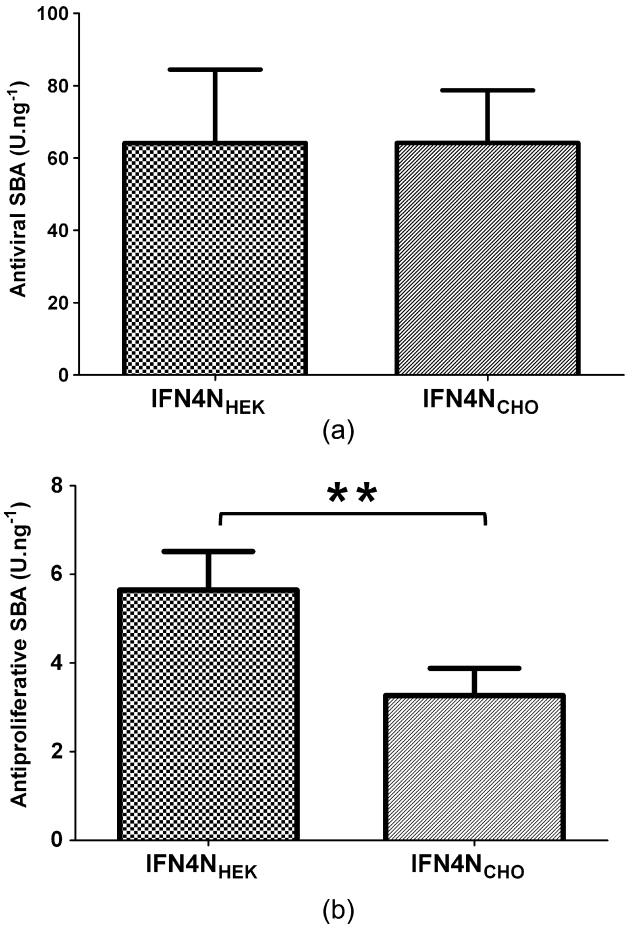

Fig. 2. *In vitro* antiviral (a) and antiproliferative (b) specific bioactivities (SBA) of $IFN4N_{CHO}$ and $IFN4N_{HEK}$. Mean ± SD is represented for each sample. The asterisk characters indicate the existence of a significant difference between the antiproliferative SBAs of the hyperglycosylated IFNs ($^{**}p = 0.001$).

Table 1
Evaluation of the ability of HEK and CHO produced IFN4N to slow the growth of tumor-derived cell lines. IC50 was calculated for cell line (ACHN, A375 and PC-3) and expressed as the media ± SD of 3 determinations.

Cell line	IC50 $IFN4N_{HEK}$ ($\mu g\ ml^{-1}$)	IC50 $IFN4N_{CHO}$ ($\mu g\ ml^{-1}$)	Ratio IC50 $IFN4N_{CHO}$/IC50 $IFN4N_{HEK}$
ACHN	1.03 ± 0.04	2.6 ± 0.8	2.5
A375	0.99 ± 0.16	1.3 ± 0.4	1.3
PC-3	0.65 ± 0.01	0.99 ± 0.13	1.5

Table 2
Monosaccharides quantification of $IFN4N_{HEK}$ and $IFN4N_{CHO}$ glycans.

Monosaccharide (mol mol IFN^{-1})	$IFN4N_{HEK}$	$IFN4N_{CHO}$
GalNAc	1.1 ± 0.3	0.8 ± 0.01
GlcNAc	13.2 ± 1.9	12.9 ± 2.5
Fuc	1.1 ± 0.4	1.6 ± 0.4
Gal	3.0 ± 0.4	11.2 ± 1.1
Man	5.1 ± 0.6	5.7 ± 0.1
Neu5Ac	4.7 ± 0.4	10.7 ± 0.6
Neu5Gc	n/d	0.12 ± 0.02

n/d = non-detectable.

This identification was carried out by comparing retention times with reference glycan standards (data not shown) and based on published work [34]. On the other hand, for $IFN4N_{HEK}$ glycans belonging to bisialylated and trisialylated groups, the most abundant peaks were the first ones of each group (considering from left to right), which would indicate a higher proportion of glycans with incomplete sialylation in comparison with the $IFN4N_{CHO}$ variant. Nevertheless, the tetrasialylated group from HEK glycans showed a similar profile to CHO glycans.

3.3.4. *N*-glycan analysis by HILIC and mass spectrometry

After labeling with 2-AB, *N*-glycans from $IFN4N_{CHO}$ and $IFN4N_{HEK}$ were analyzed by HILIC-UPLC coupled to mass spectrometry. These results are shown in Fig. 4 and the structures assigned regarding GU and mass values are summarized in Table 3. Digestions of the labeled glycans with different arrays of exoglycosidases followed by HILIC-HPLC analysis was used as a complementary study for the assignation of glycosidic structures (Fig. S1). Considering the elution positions, GU values were assigned to each of the main peaks by comparison with the dextran ladder standard for both analyses.

The predominant *N*-glycans derived from $IFN4N_{HEK}$ eluted between 5 and 8 GU values while the main structures derived from $IFN4N_{CHO}$ appeared between 8 and 14 GU. Basically, they revealed that a higher quantity of more highly-ramified complex glycans were present in the CHO-derived IFN4N while HEK glycans comprised smaller structures. It is important to note that peaks at higher GU values were detected for the glycans corresponding to $IFN4N_{HEK}$, denoting the presence of very low amounts of more branched structures (Fig. 4).

On the one hand, complete structures comprising bi-, tri- and tetra-antennary glycans with LacNAc extensions were identified for $IFN4N_{CHO}$ by mass spectrometry. Relative abundances showed that FA2G2S2, FA3G3S3, FA4G4S4 and FA4G4Lac1S4, which eluted at 47.27, 61.12, 71.77 and 77.83 min in HILIC, were the predominant structures (Table 3). Exoglycosidases digestions used as a complementary tool confirmed that all the $IFN4N_{CHO}$ glycans were core fucosylated (Fig. S1).

On the other hand, incomplete or truncated structures were the most abundant glycans detected for $IFN4N_{HEK}$. Even though some structures could not be identified by mass spectrometry, GU assignation and exoglycosydases analysis allowed their description (Fig. S1). According to the calculated relative abundances, FA2B/FA3, FA2G1 and FA2BG1 (eluting at 22.33, 25.75 and 28.93 min, respectively) were the main structures identified among HEK glycans. In this case, bisecting GlcNAc was identified, while this type of structure was not present in the CHO-derived sample (Table 3). Moreover, the exoglycosydases digestion showed that 4.5% of the *N*-glycosydic structures were non-fucosylated (ABS + BTG + JBH chromatogram for $IFN4N_{HEK}$, Fig. S1).

3.3.5. *O*-glycoprotein analysis by RP-UPLC and mass spectrometry

N-deglycosylated $IFN4N_{HEK}$ and $IFN4N_{CHO}$ were analyzed by RP-UPLC and mass spectrometry in order to study the *O*-glycosidic structures from both proteins. The molecular weight of the protein considered for the evaluation was 19,229 Da. As shown in Table 4, more heterogeneous and varied structures were detected among $IFN4N_{HEK}$, while bisialylated core 1 was the predominant *O*-glycan detected for $IFN4N_{CHO}$ (61%). As it was found for *N*-glycans, many incomplete structures were detected for $IFN4N_{HEK}$ and 49% of its *O*-glycans were neutral. In contrast, 72% of the $IFN4N_{CHO}$ *O*-glycans were bisialylated, 12% were monosialylated and only 16% were neutral.

3.4. Impact of the glycosidic content of CHO- and HEK-derived molecules in their pharmacokinetic properties

In vivo experiments were performed in Wistar rats with the aim of evaluating how the differences in the glycosylation pattern of IFN4N produced in CHO and HEK cells might affect the

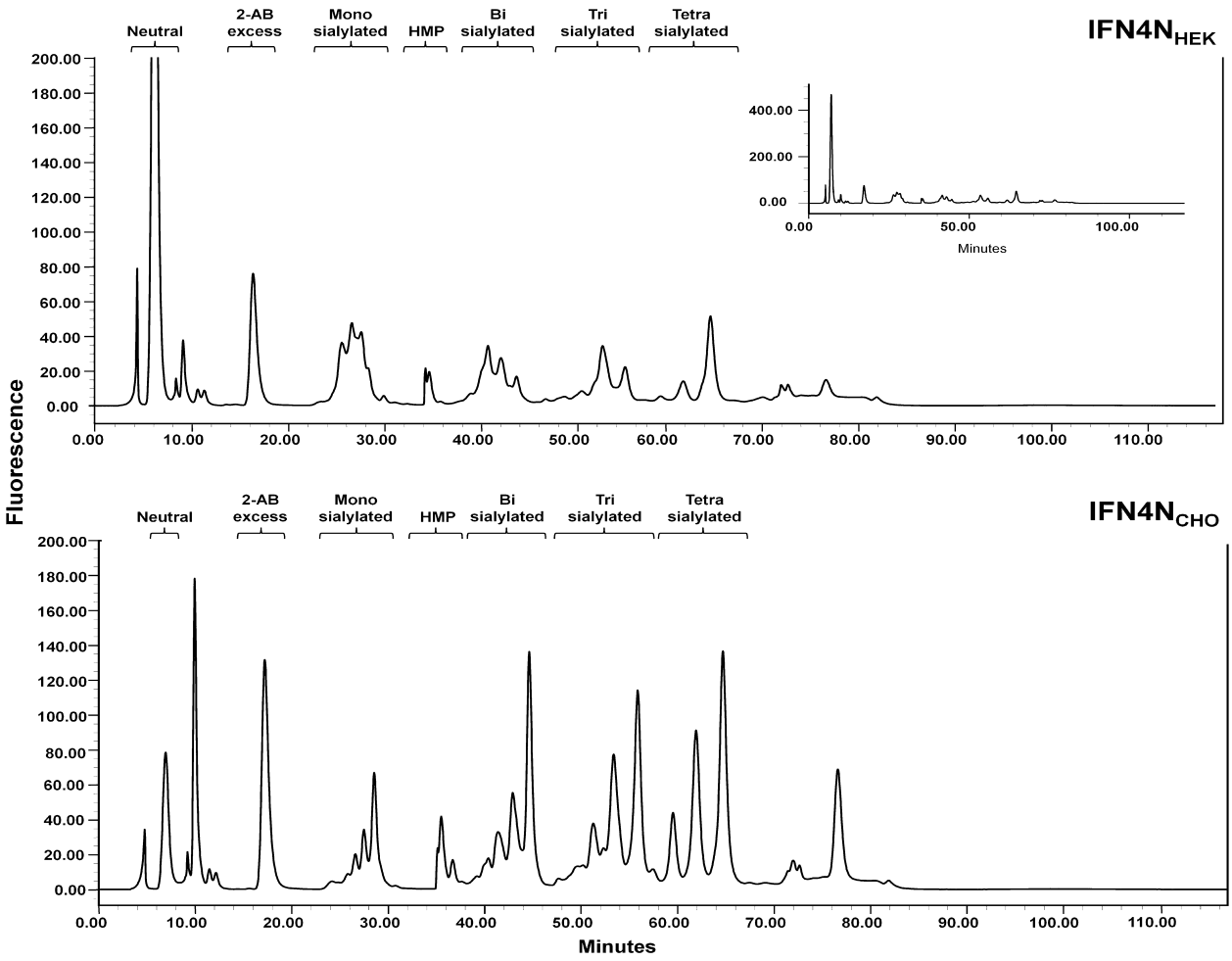

Fig. 3. WAX profiles of IFN4N$_{HEK}$ and IFN4N$_{CHO}$ 2-AB labeled *N*-glycans. Identification of neutral as well as mono, bi, tri, and tetrasialylated *N*-glycans was performed according to a fetuin standard.

pharmacokinetics of these proteins. The bioactivity profile in plasma versus time for each molecule is shown in Fig. 5 and the individual pharmacokinetic parameters are summarized in Table 5.

The main difference between both molecules was observed during the absorption phase. In fact, distribution phase was longer for IFN4N$_{CHO}$ compared to IFN4N$_{HEK}$ since T_{max} was 7.2 ± 1.3 h and 2.7 ± 0.3 h, respectively ($p = 0.03$). Moreover, the C_{max} of both proteins was significantly different, being 194 ± 17 UI ml^{-1} for IFN4N$_{CHO}$ and 149 ± 27 UI ml^{-1} for IFN4N$_{HEK}$ ($p = 0.04$). Regarding the elimination phase, no significant differences were observed between the $t_{1/2}$ ($p = 0.14$), AUC ($p = 0.052$) or CL_{app} ($p = 0.05$) of IFN4N$_{CHO}$ and IFN4N$_{HEK}$ (Table 5).

However, the values were not within the pre-defined bioequivalence criteria of 0.8–1.25 (Table S3), indicating that the pharmacokinetic parameters of IFN4N$_{CHO}$ and IFN4N$_{HEK}$ are not bioequivalent.

3.5. Antitumor effects of IFN4N$_{CHO}$ and IFN4N$_{HEK}$ in PC-3 derived solid tumors implanted in athymic nude mice

IFN4N$_{CHO}$ and IFN4N$_{HEK}$ were tested for their ability to inhibit the growth of solid tumors of prostate carcinoma-derived cells implanted in athymic nude mice.

Treatment with both proteins caused a reduction on the tumor growth rate compared to the control group (Fig. 6a). Two growth phases were identified for the control group and the group of mice treated with IFN4N$_{CHO}$. In the first one, which started on day 7 and finished on day 26, tumor growth rate was slower (42 ± 11 mm^3 · day^{-1} for the control group and 15 ± 5 mm^3 day^{-1} for the IFN IFN4N$_{CHO}$-treated group) while in the second (which comprised from day 26 until the end of the experiment), tumor volume increased more rapidly (147 ± 32 mm^3 day^{-1} for the control group and 78 ± 32 mm^3 day^{-1} for the IFN4N$_{CHO}$-treated group). In the case of IFN4N$_{HEK}$ a unique linear growth phase was identified, with a growth rate of 22 ± 5 mm^3 day^{-1}. These results showed that both proteins were able to slow the growth rate of the tumors, but IFN4N$_{HEK}$ was the most efficient one.

At the end of the experiment tumors were removed and weighed (Fig. 6b). Mean tumor weights were also significantly reduced in animals receiving IFN4N$_{CHO}$ (37% decrease, $p = 0.0184$) and IFN4N$_{HEK}$ (61% decrease, $p = 0.0009$) compared to the mean tumor weights of the PBS control group. Furthermore, this result also showed that IFN4N$_{HEK}$ was more efficient than IFN4N$_{CHO}$ as an antitumor agent in this animal model ($p = 0.0106$).

4. Discussion

Glycosylation is a wide-spread post-translational modification which has a marked influence on many properties of glycoproteins. Significant differences have been described between the glycan structures of proteins expressed in mammalian, yeast, insect and even in some bacterial systems [35]. However, much less is known

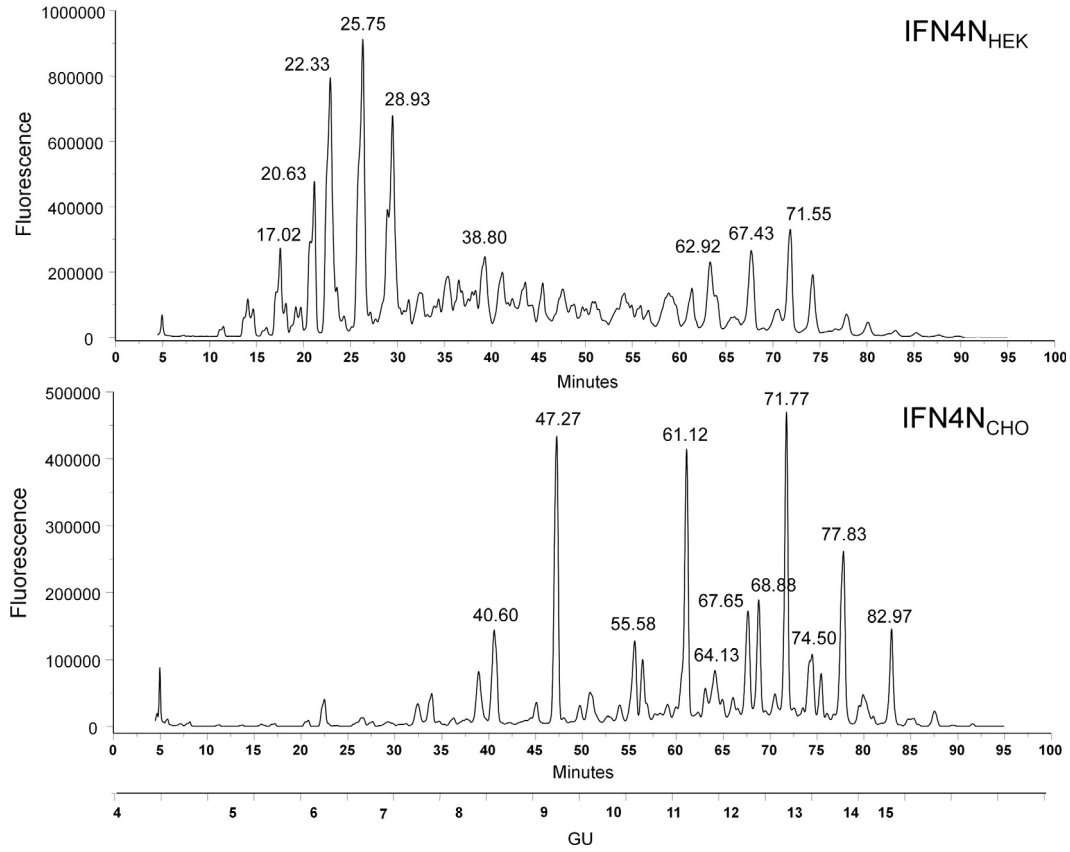

Fig. 4. HILIC-UPLC chromatograms of IFN4N$_{HEK}$ and IFN4N$_{CHO}$. Retention times of identified structures are indicated.

Table 3
Predominant *N*-glycans structures for IFN4N$_{HEK}$ e IFN4N$_{CHO}$.

Structure	GU	Observed *m/z*	Theoretical *m/z*	Error (ppm)	Abundance (%)	RT
IFN4N$_{HEK}$						
A2*	5.41	n/d	1436.476	n/d	4	17.02
FA2*	5.87	n/d	1582.534	n/d	6	20.63
FA2B/FA3	6.24	1785.657	1785.613	25	13	22.33
FA2G1*	6.70	n/d	1744.587	n/d	14	25.75
FA2BG1	7.08	1947.709	1947.666	22	13	28.93
FA2G2S1*	8.34	n/d	2197.735	n/d	4	38.80
FA4G4S2	11.65	3219.118	3219.095	7	4	62.92
FA4G4S3	12.18	3510.183	3510.190	−2	4	67.43
FA4G4S4	12.70	3801.310	3801.286	6	4	71.55
IFN4N$_{CHO}$						
FA2G2S1	8.78	2197.792	2197.735	26	5	40.60
FA2G2S2	9.11	2488.910	2488.910	0	12	47.27
FA3G3S2	10.32	2853.993	2853.963	11	4	55.58
FA3G3S3	11.14	3145.100	3145.058	13	12	61.12
FA4G4S2	11.65	3219.104	3219.095	3	4	64.13
FA4G4S3	12.18	3510.230	3510.190	11	5	67.65
FA3G3Lac1S3	12.37	3510.230	3510.190	11	5	68.88
FA4G4S4	12.70	3801.355	3801.286	18	11	71.77
FA4G4Lac1S3	13.20	3875.413	3875.322	23	5	74.50
FA4G4Lac1S4	13.77	4166.466	4166.418	12	8	77.83
FA4G4Lac4S1	15.12	4411.507	4411.600	−21	4	82.97

* Structures from IFN4N$_{HEK}$ which could not be detected (n/d) by mass spectrometry were potentially assigned considering their GU value.

about the characteristics of glycoproteins derived from different mammalian cells.

In this work, the long-lasting and hyperglycosylated hIFN-α2b mutein (IFN4N) was produced, purified and extensively characterized using two mammalian cell lines from different tissues and species: CHO-K1 (ovary, hamster) and HEK293 (kidney, human) cells. Despite the fact that the amino acidic sequences of both proteins are the same, many differences were found during their characterization.

Clear differences between the apparent molecular masses of both proteins were observed in SDS-PAGE analysis. In general, CHO-derived proteins have a higher average molecular mass compared to the same proteins produced in HEK cells [30,36], and our findings agreed with this observation. After PNGase F digestion, the

Table 4
Analysis of *O*-glycan structures from *N*-deglycosylated $IFN4N_{HEK}$ and $IFN4N_{CHO}$.

Structure	Abundance (%)	Mass (Da)	Error (Da)	Error (ppm)
$IFN4N_{HEK}$				
O-Acetyl-Nterm/HexNAc	23	19475.9	1.9	98
HexNAc	19	19431.8	−0.2	−10
HexNAc-Hex-Sial (2)	16	20176.0	0.0	0
HexNAc (2)-Hex (2)-Sial (2)	12	20542.0	3.0	147
O-Acetyl-Nterm/HexNAc (2) Hex (1)	6	19840.9	1.9	96
HexNAc (2)-Sial (2)	5	19921.3	0.7	35
HexNAc-Hex-Sial (1)	4	19885.0	0.0	0
Non-glycosylated	4	19228.0	1.0	52
HexNAc (3)-Hex (3)-Sial (1)/Oxydation M	3	20622.0	−8.0	−194
HexNAc (2)-Hex (1)-Sial (1)	2	20088.0	0.0	0
HexNAc (1)-Hex (1)	2	19590.7	−3.3	−168
Hex (1)-Sial (1)	2	19674.1	−2.9	−147
HexNAc (2)-Hex (2)-Sial (1)	1	20249.5	−5.5	−272
HexNac (2)	1	19631.7	0.7	36
$IFN4N_{CHO}$				
HexNAc-Hex-Sial (2)	61	20175.5	−0.5	
O-Acetyl-Nterm/HexNAc	14	19476.0	2	103
O-Acetyl-Nterm/HexNAc-Hex-Sial (2)	11	20216.3	−0.7	−35
HexNAc-Hex-Sial (1)	7	19884.3	−0.7	−35
HexNAc (2)-Hex (2)-Sial (1)	5	20258.3	−0.7	−35
Non-glycosylated	2	19228.0	−1	−52

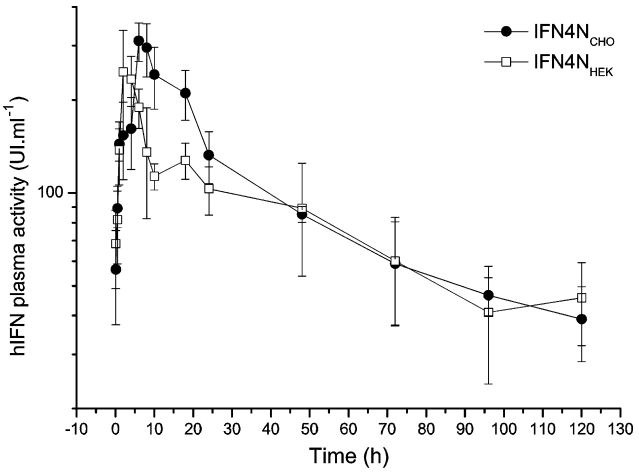

Fig. 5. Pharmacokinetic plasma profile of $IFN4N_{HEK}$ (-□-) and $IFN4N_{CHO}$ (-●-) in Wistar rats after subcutaneous administration of 2×10^5 IU of each molecule. Blood samples were collected at different time points and analyzed by antiviral activity assay. Data points are the average ± SD of four animals in each group.

N-deglycosylated proteins exhibited comparable average molecular masses, and for that reason glycosylation was confirmed as responsible for the above-mentioned disparity. This result coincided with a previous study in which 12 proteins produced in CHO and HEK cells were analyzed, noticing that disparities between most of them were due to glycosylation [28].

Glycoforms distribution analyzed by IEF showed that isoforms from $IFN4N_{CHO}$ were mainly concentrated towards the more acidic zone of the gel while those from $IFN4N_{HEK}$ were more homogeneously distributed. Thus, $IFN4N_{CHO}$ exhibited a higher proportion of acidic isoforms compared to $IFN4N_{HEK}$. A similar outcome was observed for recombinant human erythropoietin (rhEPO): while the hormone produced by CHO-K1 cells exhibited glycoforms mainly located in the low pH region (representing highly glycosylated isoforms), the one derived from HEK293 displayed a wider range of glycoforms that spread across the pH gradient [37]. Other authors reported similar differences between isoform distribution in IEF gels when the GlialCAM adhesion molecule was produced in CHO-K1 and HEK 293 cells [38]. Our IEF results agreed with sialic acid quantification, since total sialic acid content for the CHO-derived molecule was significantly higher (2.3-fold) than the corresponding one for the HEK-derived protein. This is also in agreement with what has been found in literature, since many authors have reported that glycoproteins produced in CHO-K1 cells contain a higher amount of sialic acid compared to HEK-derived proteins [2,27–29]. Importantly, an immunogenic type of sialic acid (Neu5Gc) can be incorporated as a terminal unit of the glycan structure when the glycoprotein is expressed using a non-human host, as CHO cells. Synthesis of Neu5Gc occurs by hydroxylation of the common form of human sialic acid (Neu5Ac), a reaction that is carried out by a specific enzyme that is not present in humans. Considering that humans spontaneously produce antibodies against this glycan epitope, the amounts of Neu5Gc should be controlled in order to avoid therapy failure [8,39,40]. Glycans deriving from $IFN4N_{CHO}$ contained detectable amounts of Neu5Gc, but it could not be detected in $IFN4N_{HEK}$. Consistently, Shahrokh et al. [25] reported that this antigenic sialic acid was absent in rhEPO (Dynepo™) produced by the human cell line HT-1080.

Further experiments comprising glycosydic characterization were performed to thoroughly explore the differences between the CHO- and HEK-glycosydic profiles. WAX analysis of 2-AB labeled glycans indicated the presence of more negatively charged structures (due to the presence of sialic acid) and, consequently, more branched structures for $IFN4N_{CHO}$ while neutral and monosialylated glycans were the predominant structures among

Table 5
Pharmacokinetic parameters calculated after subcutaneous administration of a single dose of 2×10^5 IU of $IFN4N_{HEK}$ and $IFN4N_{CHO}$ in rats.

	C_{max} (U ml^{-1})	T_{max} (h)	$t_{1/2}$ (h)	AUC (UI h ml^{-1})	CL_{app} (ml h^{-1})
$IFN4N_{HEK}$	149 ± 27	2.7 ± 0.3	57 ± 6	9679 ± 1206	21 ± 3
$IFN4N_{CHO}$	194 ± 17	7.2 ± 1.3	54 ± 6	11,732 ± 1115	17 ± 2

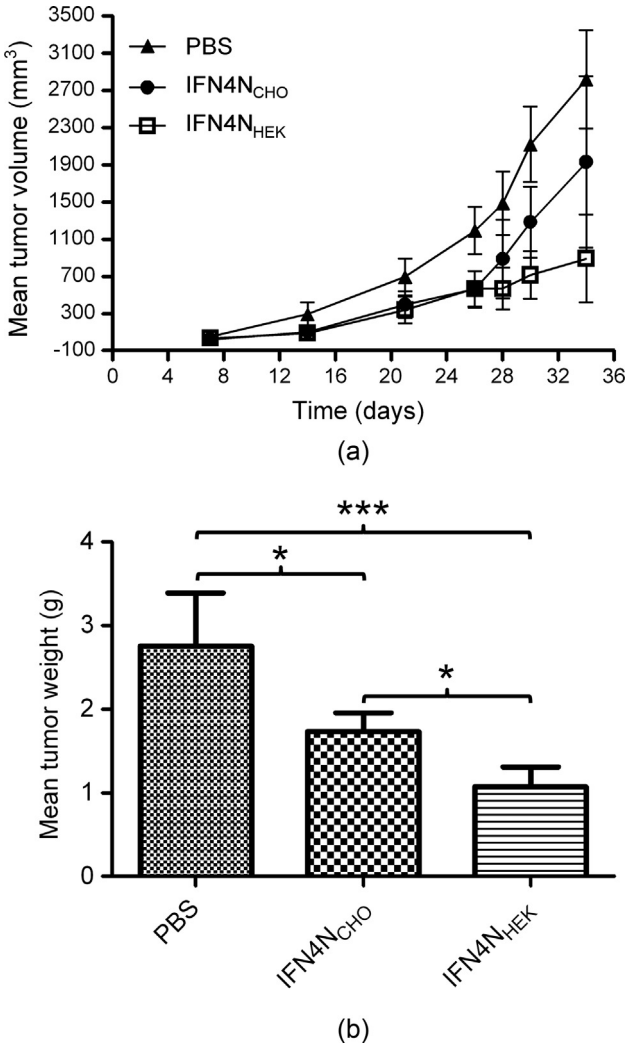

Fig. 6. *In vivo* antitumor activity of $IFN4N_{HEK}$ and $IFN4N_{CHO}$ in athymic nude mice subcutaneously implanted with 2×10^6 human prostate carcinoma PC-3 cells. Mice (n = 6) were treated with 5 μg of each protein. A control group received PBS injections. Tumor size was measured every week prior to treatment. The mean tumor volume ± SD over time is shown in (a). At the end of the experiment, tumors were excised and weighed. The mean tumor weight ± SD is shown in (b).

HEK glycans. Accordingly, many authors have previously described that CHO cells-derived glycoproteins evidence more sialylated glycans compared to molecules produced in HEK293, such as human thyrotropin (hTSH) and soluble intracellular adhesion molecule-1 (sICAM-1) [41–43] or than molecules purified from native tissues as the human prolactin (hPRL) obtained from pituitary material [44].

The analysis of the 2-AB labeled glycans by HILIC and mass spectrometry also showed differences for the HEK- and CHO-produced IFN4N. On the one hand, complex structures of high GU and high *m/z* values could be identified for glycans derived from $IFN4N_{CHO}$, mainly comprising tri- and tetraantennary structures with LacNac extensions. On the other hand, simpler and truncated structures with low GU and *m/z* values were the main components of $IFN4N_{HEK}$ glycans. Consistently, different Erythropoiesis Stimulating Agents (ESAs) produced in CHO cells contained LacNac extensions in some structures while this repeated glycan unit was present in considerably fewer amounts in Dynepo™ [25]. Moreover, glycans isolated from HEK293-derived protease inhibitor alpha-1-antitrypsin (A1AT) were mainly biantennary structures while no tetraantennary structures were detected [45]. The same result was shown by Böhm et al. who produced recombinant Factor VII (rFVII) in HEK 293 cells, and they did not observe tri- or tetraantennary structures among its glycans either [46]. In this way, despite having different sequence and structure around the *N*-glycosylation site, the CHO and HEK glycosylation patterns of other proteins seem to be consistent with those observed for the hyperglycosylated IFN mutein. Thereby, different studies agree with the fact that HEK-derived glycoproteins comprise smaller, less-branched glycan structures regarding those derived from CHO cells. Exoglycosydases digestions were useful in order to complete and confirm the study made by mass spectrometry.

In accordance with our previous findings, monosaccharides quantification showed the presence of a significantly higher content of galactose for $IFN4N_{CHO}$ compared to $IFN4N_{HEK}$ glycans. Again, this result supports the hypothesis of considerable differences between the branching levels of glycans derived from the two cell lines, and also shows that truncated glycans from HEK cells mainly end in an *N*-acetylglucosamine residue.

The notable disparities between the glycosydic profiles of both IFN4N molecules prompted us to think that extensive differences might exist between their pharmacokinetic profiles. Studies performed in rats evidenced differences during the absorption phase, since $IFN4N_{CHO}$ was 3-times delayed to reach the maximum plasma concentration, which was also significantly different in comparison with that of $IFN4N_{HEK}$. Nevertheless, the $t_{1/2}$, CL_{app} and AUC did not differ notably between both proteins. Although many authors have previously described that a higher glycosylation degree contributes positively to the pharmacokinetic properties of therapeutic glycoproteins [47,48], the understanding of the pharmacokinetic behavior of each molecule seems to be much more complicated.

Previous studies have postulated that proteins with galactose as terminating glycan (non-sialylated or desialylated proteins) undergo a fast removal from the circulation through endocytosis mediated by the asialoglycoprotein receptors expressed in the hepatocytes [49]. Besides, it has been demonstrated that glycoproteins with mannose-, N-acetylglucosamine-, or fucose-terminated glycans could be also removed from the circulation due to specific interactions with other mammalian lectin-like receptors expressed in different cell types. Importantly, some authors have demonstrated that depending on their glycosylation patterns glycoproteins could be targeted to certain tissue types and organs [27,50–52]. Thus, differences in the glycosydic structures of $IFN4N_{CHO}$ and $IFN4N_{HEK}$ might also direct these proteins through different pathways and allow or interfere the interaction with the corresponding receptors.

A similar reasoning could be applied in order to analyze the *in vitro* biological behavior of both IFN4N molecules. On the one hand, both glycoproteins exhibited a higher antiviral SBA compared to their corresponding antiproliferative SBA. This behavior might be explained by the fact that a strong ligand receptor interaction is necessary for the growth inhibitory response, while the antiviral state can be induced even when the binding is weak [53]. On the other hand, while no differences between the antiviral activities of both glycoproteins were detected, $IFN4N_{HEK}$ exhibited a remarkably higher antiproliferative activity than $IFN4N_{CHO}$. This may suggest that differences in the glycosylation could affect the binding of the molecule to its receptor, affecting the antiproliferative activity which, as it has been mentioned above, is more sensitive to changes in the binding affinity compared to the antiviral action [54]. As it was demonstrated for EPO, the rule seems to be that the lower the amount of sialic acid, the higher the *in vitro* activity [55]. Other report showed that hTSH was more active if produced in CHO Lec2 cell line (deficient for the production of sialic acid oligosaccharides) than CHO normal cells. Moreover, after neuraminidase digestion, $hTSH_{CHO}$ increased its *in vitro* activity

to an EC50 similar to the CHO Lec2-expressed hTSH. Also, it was shown that hTSH was six 6-times more active if expressed in HEK 293 cells than the CHO-derived one [41]. Aiming to confirm the higher antiproliferative SBA of $IFN4N_{HEK}$ compared to that of $IFN4N_{CHO}$, another three human tumor-derived cell lines were used for *in vitro* experiments. Once more, $IFN4N_{HEK}$ showed a better antiproliferative activity compared to $IFN4N_{CHO}$, verifying that the less sialylated variant exhibits a higher binding affinity for the receptor which translates into a stronger signal transduction, and, consequently, to a more potent growth-inhibitory action [56]. Moreover, *in vivo* studies demonstrated that the HEK-derived IFN4N was able to slow down the growth rate of human prostate tumors implanted in nude mice more efficiently than protein produced in CHO cells. In this context, glycosylation performed by HEK cells seems to lean the scale towards a better *in vitro* activity that results in an improved *in vivo* efficacy of the therapeutic protein IFN4N.

To summarize, in this work we postulate two different therapeutic candidates expressed in different host cells whose main molecular difference lies in their glycosylation profile. Both $IFN4N_{CHO}$ and $IFN4N_{HEK}$ seem to be suitable candidates for the treatment of viral infections since they demonstrate similar *in vitro* antiviral SBA. However, the significantly higher *in vitro* antiproliferative SBA displayed by the HEK-derived molecule allows us to postulate this protein as a potential therapeutic agent for anti-tumor therapies. Indeed, *in vivo* antitumor activity assays demonstrated that $IFN4N_{HEK}$ was more efficient than $IFN4N_{CHO}$, despite no significant differences were found in the Cl_{app} between both proteins.

In conclusion, this report suggests that an extensive research should be done in order to select an appropriate host to set up a new bioprocess, and encourage the use of HEK293 cells for the production of a novel hyperglycosylated biopharmaceutical.

Conflict of interest

The authors declare that they have no conflict of interests.

Acknowledgements

The authors thank Gustavo Orozco for his help in pharmacokinetic experiments, Marilin Rey, Lorena Lagger and Cecilia Lubo for their contribution in glycosylation analysis, Gisela Leal for meticulously proofreading the manuscript, Gustavo Vazquez y Máximo Barreras for mass spectrometry analysis of *N*-glycans and *O*-glycoprotein and Sebastian Antuña for figures editing.

This work was supported by the following Argentine institutions: Universidad Nacional del Litoral (C.A.I.+D. 2013-2016 PJ No. 500 201101 00022 LI and No. PI 501 201101 00313 LI; SAT No. 356.698), Zelltek SA and Agencia Nacional de Promoción Científica y Tecnológica (ANPCyT-FONCyT; PICT 2012-2015, No. 1575). NC, RK and MO are research members of Consejo Nacional de Investigaciones Científicas y Técnicas (CONICET). AG has received a fellowship from CONICET.

Appendix A. Supplementary material

Supplementary data associated with this article can be found, in the online version, at http://dx.doi.org/10.1016/j.ejpb.2016.11.012.

References

[1] K. Mariño, J. Bones, J.J. Kattla, P.M. Rudd, A systematic approach to protein glycosylation analysis: a path through the maze, Nat. Chem. Biol. 6 (2010) 713–723.
[2] M. Butler, M. Spearman, The choice of mammalian cell host and possibilities for glycosylation engineering, Curr. Opin. Biotechnol. 30 (2014) 107–112.
[3] M. De Jesus, F.M. Wurm, Manufacturing recombinant proteins in kg-ton quantities using animal cells in bioreactors, Eur. J. Pharm. Biopharm. 78 (2011) 184–188.
[4] Y. Durocher, M. Butler, Expression systems for therapeutic glycoprotein production, Curr. Opin. Biotechnol. 20 (2009) 700–707.
[5] J. Dumont, D. Euwart, B. Mei, S. Estes, R. Kshirsagar, Human cell lines for biopharmaceutical manufacturing: history, status, and future perspectives, Crit. Rev. Biotechnol. (2015) 1–13.
[6] C.J. Bosques, B.E. Collins, J.W. Meador 3rd, H. Sarvaiya, J.L. Murphy, G. Dellorusso, D.A. Bulik, I.H. Hsu, N. Washburn, S.F. Sipsey, J.R. Myette, R. Raman, Z. Shriver, R. Sasisekharan, G. Venkataraman, Chinese hamster ovary cells can produce galactose-alpha-1,3-galactose antigens on proteins, Nat. Biotechnol. 28 (2010) 1153–1156.
[7] S. Dietmair, M.P. Hodson, L.E. Quek, N.E. Timmins, P. Gray, L.K. Nielsen, A multi-omics analysis of recombinant protein production in Hek293 cells, PLoS ONE 7 (2012) e43394.
[8] D. Ghaderi, M. Zhang, N. Hurtado-Ziola, A. Varki, Production platforms for biotherapeutic glycoproteins. Occurrence, impact, and challenges of non-human sialylation, Biotechnol. Genet. Eng. Rev. 28 (2012) 147–175.
[9] D. Ghaderi, R.E. Taylor, V. Padler-Karavani, S. Diaz, A. Varki, Implications of the presence of N-glycolylneuraminic acid in recombinant therapeutic glycoproteins, Nat. Biotechnol. 28 (2010) 863–867.
[10] V. Padler-Karavani, H. Yu, H. Cao, H. Chokhawala, F. Karp, N. Varki, X. Chen, A. Varki, Diversity in specificity, abundance, and composition of anti-Neu5Gc antibodies in normal humans: potential implications for disease, Glycobiology 18 (2008) 818–830.
[11] S. Goodbourn, L. Didcock, R.E. Randall, Interferons: cell signalling, immune modulation, antiviral response and virus countermeasures, J. Gen. Virol. 81 (2000) 2341–2364.
[12] S. Pestka, The interferons: 50 years after their discovery, there is much more to learn, J. Biol. Chem. 282 (2007) 20047–20051.
[13] E.C. Borden, G.C. Sen, G. Uze, R.H. Silverman, R.M. Ransohoff, G.R. Foster, G.R. Stark, Interferons at age 50: past, current and future impact on biomedicine, Nat. Rev. Drug Discov. 6 (2007) 975–990.
[14] N.A. El-Baky, E.M. Redwan, Therapeutic alpha-interferons protein: structure, production, and biosimilar, Prep. Biochem. Biotechnol. 45 (2015) 109–127.
[15] R.E. Kontermann, Strategies for extended serum half-life of protein therapeutics, Curr. Opin. Biotechnol. 22 (2011) 868–876.
[16] N. Ceaglio, M. Etcheverrigaray, R. Kratje, M. Oggero, Novel long-lasting interferon alpha derivatives designed by glycoengineering, Biochimie 90 (2008) 437–449.
[17] A. Gugliotta, M. Oggero-Eberhardt, M. Etcheverrigaray, R. Kratje, N. Ceaglio, Differences in the production of hyperglycosylated IFN alpha in CHO and HEK 293 cells, BMC Proc. 7 (Suppl. 6) (2013) P33.
[18] M. Depetris, P. Casalis, R. Kratje, M. Etcheverrigaray, M. Oggero, A scFv antibody fragment as a therapeutic candidate to neutralize a broad diversity of human IFN-alpha subtypes, J. Immunol. Meth. 334 (2008) 104–113.
[19] N. Ceaglio, A. Gugliotta, M.B. Tardivo, D. Cravero, M. Etcheverrigaray, R. Kratje, M. Oggero, Improvement of in vitro stability and pharmacokinetics of hIFN-alpha by fusing the carboxyl-terminal peptide of hCG beta-subunit, J. Biotechnol. 221 (2016) 13–24.
[20] P.C. Familletti, S. Rubinstein, S. Pestka, A convenient and rapid cytopathic effect inhibition assay for interferon, Meth. Enzymol. 78 (1981) 387–394.
[21] T. Nederman, E. Karlstrom, L. Sjodin, An in vitro bioassay for quantitation of human interferons by measurements of antiproliferative activity on a continuous human lymphoma cell line, Biologicals 18 (1990) 29–34.
[22] M. Butler, D. Quelhas, A.J. Critchley, H. Carchon, H.F. Hebestreit, R.G. Hibbert, L. Vilarinho, E. Teles, G. Matthijs, E. Schollen, P. Argibay, D.J. Harvey, R.A. Dwek, J. Jaeken, P.M. Rudd, Detailed glycan analysis of serum glycoproteins of patients with congenital disorders of glycosylation indicates the specific defective glycan processing step and provides an insight into pathogenesis, Glycobiology 13 (2003) 601–622.
[23] G.R. Guile, P.M. Rudd, D.R. Wing, S.B. Prime, R.A. Dwek, A rapid high-resolution high-performance liquid chromatographic method for separating glycan mixtures and analyzing oligosaccharide profiles, Anal. Biochem. 240 (1996) 210–226.
[24] L. Royle, M.P. Campbell, C.M. Radcliffe, D.M. White, D.J. Harvey, J.L. Abrahams, Y.G. Kim, G.W. Henry, N.A. Shadick, M.E. Weinblatt, D.M. Lee, P.M. Rudd, R.A. Dwek, HPLC-based analysis of serum N-glycans on a 96-well plate platform with dedicated database software, Anal. Biochem. 376 (2008) 1–12.
[25] Z. Shahrokh, L. Royle, R. Saldova, J. Bones, J.L. Abrahams, N.V. Artemenko, S. Flatman, M. Davies, A. Baycroft, S. Sehgal, M.W. Heartlein, D.J. Harvey, P.M. Rudd, Erythropoietin produced in a human cell line (Dynepo) has significant differences in glycosylation compared with erythropoietins produced in CHO cell lines, Mol. Pharm. 8 (2010) 286–296.
[26] L. Shargel, S. Wu-Pong, A.B.C. Yu, Applied Biopharmaceutics & Pharmacokinetics, Appleton & Lange Reviews/McGraw-Hill, Medical Pub. Division, New York, 2005.
[27] R.J. Sola, K. Griebenow, Glycosylation of therapeutic proteins: an effective strategy to optimize efficacy, BioDrugs 24 (2010) 9–21.
[28] A. Croset, L. Delafosse, J.P. Gaudry, C. Arod, L. Glez, C. Losberger, D. Begue, A. Krstanovic, F. Robert, F. Vilbois, L. Chevalet, B. Antonsson, Differences in the glycosylation of recombinant proteins expressed in HEK and CHO cells, J. Biotechnol. 161 (2012) 336–348.

[29] E.P. Go, H.X. Liao, S.M. Alam, D. Hua, B.F. Haynes, H. Desaire, Characterization of host-cell line specific glycosylation profiles of early transmitted/founder HIV-1 gp120 envelope proteins, J. Proteome Res. 12 (2013) 1223–1234.
[30] K.F. Suen, M.S. Turner, F. Gao, B. Liu, A. Althage, A. Slavin, W. Ou, E. Zuo, M. Eckart, T. Ogawa, M. Yamada, T. Tuntland, J.L. Harris, J.W. Trauger, Transient expression of an IL-23R extracellular domain Fc fusion protein in CHO vs. HEK cells results in improved plasma exposure, Protein Expr. Purif. 71 (2010) 96–102.
[31] M. Gary-Bobo, P. Nirde, A. Jeanjean, A. Morere, M. Garcia, Mannose 6-phosphate receptor targeting and its applications in human diseases, Curr. Med. Chem. 14 (2007) 2945–2953.
[32] G. Grampp, S. Ramanan, The diversity of biosimilar design and development: implications for policies and stakeholders, BioDrugs 29 (2015) 365–372.
[33] N. Ceaglio, M. Etcheverrigaray, H.S. Conradt, N. Grammel, R. Kratje, M. Oggero, Highly glycosylated human alpha interferon: an insight into a new therapeutic candidate, J. Biotechnol. 146 (2010) 74–83.
[34] E. Llop, R. Gutierrez-Gallego, J. Segura, J. Mallorqui, J.A. Pascual, Structural analysis of the glycosylation of gene-activated erythropoietin (epoetin delta, Dynepo), Anal. Biochem. 383 (2008) 243–254.
[35] S.A. Brooks, Protein glycosylation in diverse cell systems: implications for modification and analysis of recombinant proteins, Expert Rev. Proteomics 3 (2006) 345–359.
[36] M. Wang, T. Ishino, A. Joyce, A. Tam, W. Duan, L. Lin, W.S. Somers, R. Kriz, D.M. O'Hara, Faster in vivo clearance of human embryonic kidney than Chinese hamster ovary cell derived protein: role of glycan mediated clearance, J. Biosci. Bioeng. 119 (2015) 657–660.
[37] P. Zhang, D.L. Tan, D. Heng, T. Wang, Mariati, Y. Yang, Z. Song, A functional analysis of N-glycosylation-related genes on sialylation of recombinant erythropoietin in six commonly used mammalian cell lines, Metab. Eng. 12 (2010) 526–536.
[38] J.P. Gaudry, C. Arod, C. Sauvage, S. Busso, P. Dupraz, R. Pankiewicz, B. Antonsson, Purification of the extracellular domain of the membrane protein GlialCAM expressed in HEK and CHO cells and comparison of the glycosylation, Protein Expr. Purif. 58 (2008) 94–102.
[39] N. Jenkins, R.B. Parekh, D.C. James, Getting the glycosylation right: implications for the biotechnology industry, Nat. Biotechnol. 14 (1996) 975–981.
[40] M. Takahashi, Y. Kuroki, K. Ohtsubo, N. Taniguchi, Core fucose and bisecting GlcNAc, the direct modifiers of the N-glycan core: their functions and target proteins, Carbohydr. Res. 344 (2009) 1387–1390.
[41] M. Grossmann, M.W. Szkudlinski, J.E. Tropea, L.A. Bishop, N.R. Thotakura, P.R. Schofield, B.D. Weintraub, Expression of human thyrotropin in cell lines with different glycosylation patterns combined with mutagenesis of specific glycosylation sites. Characterization of a novel role for the oligosaccharides in the in vitro and in vivo bioactivity, J. Biol. Chem. 270 (1995) 29378–29385.
[42] J.W. Bloom, M.S. Madanat, M.K. Ray, Cell line and site specific comparative analysis of the N-linked oligosaccharides on human ICAM-1des454-532 by electrospray ionization mass spectrometry, Biochemistry 35 (1996) 1856–1864.
[43] V.I. Otto, T. Schurpf, G. Folkers, R.D. Cummings, Sialylated complex-type N-glycans enhance the signaling activity of soluble intercellular adhesion molecule-1 in mouse astrocytes, J. Biol. Chem. 279 (2004) 35201–35209.
[44] M.V. Capone, M.F. Suzuki, J.E. Oliveira, R. Damiani, C.R. Soares, P. Bartolini, N-glycoprofiling analysis in a simple glycoprotein model: a comparison between recombinant and pituitary glycosylated human prolactin, J. Biotechnol. 202 (2015) 78–87.
[45] J. Rosenlocher, G. Sandig, C. Kannicht, V. Blanchard, S.O. Reinke, S. Hinderlich, Recombinant glycoproteins: the impact of cell lines and culture conditions on the generation of protein species, J. Proteomics 134 (2016) 85–92.
[46] E. Bohm, B.K. Seyfried, M. Dockal, M. Graninger, M. Hasslacher, M. Neurath, C. Konetschny, P. Matthiessen, A. Mitterer, F. Scheiflinger, Differences in N-glycosylation of recombinant human coagulation factor VII derived from BHK, CHO, and HEK293 cells, BMC Biotechnol. 15 (2015) 87.
[47] A.R. Costa, M.E. Rodrigues, M. Henriques, R. Oliveira, J. Azeredo, Glycosylation: impact, control and improvement during therapeutic protein production, Crit. Rev. Biotechnol. 34 (2013) 281–299.
[48] A.M. Sinclair, S. Elliott, Glycoengineering: the effect of glycosylation on the properties of therapeutic proteins, J. Pharm. Sci. 94 (2005) 1626–1635.
[49] A.G. Morell, G. Gregoriadis, I.H. Scheinberg, J. Hickman, G. Ashwell, The role of sialic acid in determining the survival of glycoproteins in the circulation, J. Biol. Chem. 246 (1971) 1461–1467.
[50] V. Bocci, F. Carraro, A. Naldini, P.P. Cagol, E.M. Pasqual, C. Prevaldi, D. Casara, Distribution of human recombinant interferon-alpha 2 in rat plasma, liver, and experimental liver metastases, Mol. Biother. 2 (1990) 233–234.
[51] I. Mahmood, M.D. Green, Pharmacokinetic and pharmacodynamic considerations in the development of therapeutic proteins, Clin. Pharmacokinet. 44 (2005) 331–347.
[52] F. Higel, A. Seidl, F. Sorgel, W. Friess, N-glycosylation heterogeneity and the influence on structure, function and pharmacokinetics of monoclonal antibodies and Fc fusion proteins, Eur. J. Pharm. Biopharm. 100 (2016) 94–100.
[53] J. Ghislain, G. Sussman, S. Goelz, L.E. Ling, E.N. Fish, Configuration of the interferon-alpha/beta receptor complex determines the context of the biological response, J. Biol. Chem. 270 (1995) 21785–21792.
[54] C. Thomas, I. Moraga, D. Levin, P.O. Krutzik, Y. Podoplelova, A. Trejo, C. Lee, G. Yarden, S.E. Vleck, J.S. Glenn, G.P. Nolan, J. Piehler, G. Schreiber, K.C. Garcia, Structural linkage between ligand discrimination and receptor activation by type I interferons, Cell 146 (2011) 621–632.
[55] M. Goto, K. Akai, A. Murakami, C. Hashimoto, E. Tsuda, M. Ueda, G. Kawanishi, N. Takahashi, A. Ishimoto, H. Chiba, R. Sasaki, Production of recombinant human erythropoietin in mammalian cells: host-cell dependency of the biological activity of the cloned glycoprotein, Nat. Biotechnol. 6 (1988) 67–71.
[56] E. Jaks, M. Gavutis, G. Uze, J. Martal, J. Piehler, Differential receptor subunit affinities of type I interferons govern differential signal activation, J. Mol. Biol. 366 (2007) 525–539.